Ann Nucl Med (2014) 28:860–873
DOI 10.1007/s12149-014-0881-2

ORIGINAL ARTICLE

Evaluation of a direct 4D reconstruction method using generalised linear least squares for estimating nonlinear micro-parametric maps

Georgios I. Angelis · Julian C. Matthews · Fotis A. Kotasidis · Pawel J. Markiewicz · William R. Lionheart · Andrew J. Reader

Received: 14 January 2014 / Accepted: 1 July 2014 / Published online: 30 July 2014
© The Japanese Society of Nuclear Medicine 2014

Abstract
Objective Estimation of nonlinear micro-parameters is a computationally demanding and fairly challenging process, since it involves the use of rather slow iterative nonlinear fitting algorithms and it often results in very noisy voxel-wise parametric maps. Direct reconstruction algorithms can provide parametric maps with reduced variance, but usually the overall reconstruction is impractically time consuming with common nonlinear fitting algorithms.
Methods In this work we employed a recently proposed direct parametric image reconstruction algorithm to estimate the parametric maps of all micro-parameters of a two-tissue compartment model, used to describe the kinetics of [^{18}F]FDG. The algorithm decouples the tomographic and the kinetic modelling problems, allowing the use of previously developed post-reconstruction methods, such as the generalised linear least squares (GLLS) algorithm.
Results Results on both clinical and simulated data showed that the proposed direct reconstruction method provides considerable quantitative and qualitative improvements for all micro-parameters compared to the conventional post-reconstruction fitting method. Additionally, region-wise comparison of all parametric maps against the well-established filtered back projection followed by post-reconstruction non-linear fitting, as well as the direct Patlak method, showed substantial quantitative agreement in all regions.
Conclusions The proposed direct parametric reconstruction algorithm is a promising approach towards the estimation of all individual microparameters of any compartment model. In addition, due to the linearised nature of the GLLS algorithm, the fitting step can be very efficiently implemented and, therefore, it does not considerably affect the overall reconstruction time.

Keywords PET reconstruction · Parametric imaging · GLLS · Kinetic modelling

G. I. Angelis (✉)
Faculty of Health Sciences and Brain and Mind Research Institute, The University of Sydney, Sydney, NSW 2006, Australia
e-mail: georgios.angelis@sydney.edu.au

G. I. Angelis · J. C. Matthews · F. A. Kotasidis · P. J. Markiewicz
Wolfson Molecular Imaging Centre, MAHSC, The University of Manchester, Manchester M20 3LJ, UK

F. A. Kotasidis
Division of Nuclear Medicine and Molecular Imaging, Geneva University Hospital, University of Geneva, Geneva, Switzerland

W. R. Lionheart
Department of Mathematics, The University of Manchester, Manchester, UK

A. J. Reader
King's College London, Lambeth Wing, St Thomas' Hospital, London SE1 7EH, UK

A. J. Reader
Montreal Neurological Institute, McGill University, Montreal, Canada

Introduction

Meaningful physiological parameters about tissues of interest can be extracted using dynamic positron emission tomography (PET) data. Conventional approaches generate these kinetic parameters from the independently reconstructed time frames, after fitting the regional time–activity curves (TACs) to an appropriate kinetic model [1–3]. Most

of these kinetic models are based on the utilisation of compartments to describe the behaviour of the tracer within the tissue of interest. Each compartment identifies either a distinct possible location or a different chemical state of the tracer within the same place. The constant rates of the transfer of the tracer between different compartments comprise the parameters of the model that have physiological meaning and are estimated by nonlinear least squares (NLLS) optimisation algorithms [4, 5].

Although it would be preferable to estimate the kinetic parameters at the voxel level to enhance characterisation of the regional heterogeneity, conventional approaches pose two severe limitations. The first limitation is that voxel-level TACs are usually extremely noisy, which makes it almost impossible to acquire reliable parameter estimates using nonlinear optimisation procedures, since they are often unstable and converge to local minima if the initial parameter estimate is not appropriate (i.e. close to the global maximum). However, this limitation is often overcome by post-smoothing the reconstructed images using a Gaussian kernel, before the application of the kinetic model. Although this approach can lead to improved parameter estimation it comes at the expense of reduced resolution in the parametric images and increased heterogeneity within the voxel, which the kinetic model being used might not adequately model.

The second limitation is that well-established nonlinear optimisation procedures, such as the Levenberg–Marquardt (LM) [6], are fairly computationally intensive. Although they are very powerful, since they can estimate all individual parameters from any compartment model with minimal bias, they cannot be used to estimate the kinetic parameters at the voxel level, as this would be an unrealistically long effort. To account for this limitation, graphical analysis techniques [7, 8] have been proposed, which transform the dynamic data into a set of linear equations that are efficiently solved using fast linear regression [9]. In addition, this transformation leads to fewer parameters to be optimised, which allows for improved, efficient and reliable parameter estimation with a small standard error due to the employed assumptions during the linearisation [10, 11].

Reconstruction of parametric maps directly from the measured projection data has attracted increased attention over the recent years, since it has the potential to provide estimates with improved statistical quality (both in terms of accuracy and precision). The main advantage of such approaches is that the kinetic model is applied directly on the raw measured data, where the noise statistics can be well modelled as Poisson and thus leading to statistically more efficient parameter estimates.

Over the previous years many groups have proposed different methods for estimating the parametric maps directly from the measured data (for reviews see [12, 13]). Some of them have focused on the estimation of linear kinetic parameters based either on a spectral analysis model [14–16], or on graphical analysis methods, such as the Patlak [17–19] and the Logan plots [20]. These approaches have been successfully applied on clinical data, leading to fast and efficient calculation of parametric maps. However, the downside of such approaches is that, due to the linear transformation, they can only provide macro-parameters of interest, such as the uptake rate K_i and the volume of distribution V_D.

An alternative to linear kinetic models is the use of nonlinear kinetic models (i.e. a mixture of exponentials). These approaches allow the estimation of individual kinetic parameters, but due to the coupling between the reconstruction and the nonlinear parameter estimation, they tend to be computationally impractical, forcing Kamasak et al. [21] to employ a multi-resolution grid technique to accelerate convergence. On the other hand, Wang and Qi [22] proposed a generalised reconstruction method, based on the optimisation transfer framework, to decouple the reconstruction problem from the nonlinear kinetic fitting, allowing well-established least squares optimisation procedures to be used. Although this approach is applicable to any kinetic model, the use of nonlinear regression procedures, such as the LM algorithm, during the parameter estimation step, pose a significant limitation towards the application of the method to clinical data. This is especially true for images obtained from the High Resolution Research Tomograph (HRRT), where a typical brain occupies approximately 2.5–3 million voxels in the reconstructed image and, therefore, reconstruction of voxel-wise parametric maps would be almost impossible.

Matthews et al. [23] proposed a generalised extension of existing methods [16, 22], which is applicable to any spatiotemporal model. Through an expectation maximisation (EM) framework the original spatiotemporal 4D problem can be reduced to an image-based maximum likelihood (ML) problem or to an equivalent least squares (LS) problem, where the weights are determined based on a one-step-late approach. Therefore, fast and efficient image-based techniques, such as the generalised linear least squares (GLLS) [24] or the preconditioned conjugate gradient (PCG) [16], can be used to optimise the LS or the ML the objective function, respectively, leading to fast convergence characteristics, as well as practical reconstruction times.

To the best of our knowledge there has been no study that applied a direct reconstruction algorithm on real clinical data to estimate all individual kinetic parameters of a two-tissue compartment model. Therefore, in this work we extend the method proposed by Matthews et al. [23] to estimate all individual micro-parameters of a nonlinear

kinetic model, which forms one of the key novelties of this work. In addition, an important novelty and differentiation from existing methods is that the kinetic parameters are estimated within the GLLS framework, where the linearised nature of the fitting problem makes micro-parameter estimation computationally more practical. The effectiveness of the proposed method over the conventional post-reconstruction kinetic parameter estimation, is demonstrated by means of a 4D simulation and clinical [^{18}F]FDG brain data obtained on the HRRT scanner.

Theory

Dynamic data model

The measured dynamic PET data, $\mathbf{m} = \{m_{fi}\} \in \mathbb{R}^{T\times M}$, where T is the total number of dynamic frames and M the total number of sinogram bins, are usually modelled as a collection of statistically independent Poisson variables:

$$m_{fi} \sim \text{Poisson}\ \{\bar{y}_{fi}\}, \qquad \forall f, i, \tag{1}$$

with the mean expected data $\bar{\mathbf{y}} = \{\bar{y}_{fi}\} \in \mathbb{R}^{T\times M}$ being linearly related to the unknown tracer distribution $\bar{\mathbf{x}} = \{\bar{x}_{fj}\} \in \mathbb{R}^{T\times N}$ (where N is the total number of image voxels) via the following affine transformation:

$$\bar{y}_{fi} = \sum_j p_{ij}\bar{x}_{fj} + n_{fi}, \qquad \forall f, i, \tag{2}$$

where $\mathbf{p} = \{p_{ij}\} \in \mathbb{R}^{M\times N}$ is the known probability that a photon pair emitted from the jth image voxel will be detected at the ith projection bin and $\mathbf{n} = \{n_{fi}\} \in \mathbb{R}^{T\times M}$ represents the mean background events (i.e. randoms and scatter) detected in the ith projection bin, during the fth time frame.

Kinetic model

Conventionally, the kinetic behaviour of [^{18}F]FDG in the target tissue, $C_{\mathrm{T}}(t)$, is described by a two-tissue compartment model, which consists of the concentration of the 'free' [^{18}F]FDG in tissue, C_{F}, and the phosphorylated (bound) FDG $-$ 6 $-$ PO$_4$ in tissue, $C_{\mathrm{B}}(t)$. The transfer of the tracer between compartments is represented by a set of first order differential equations [2]:

$$\frac{\mathrm{d}}{\mathrm{d}t}C_{\mathrm{F}}(t) = K_1 C_{\mathrm{p}}(t) - (k_2 + k_3)C_{\mathrm{F}}(t) + k_4 C_{\mathrm{B}}(t) \tag{3}$$

$$\frac{\mathrm{d}}{\mathrm{d}t}C_{\mathrm{B}}(t) = k_3 C_{\mathrm{F}}(t) - k_4 C_{\mathrm{B}}(t) \tag{4}$$

where $C_{\mathrm{p}}(t)$ is the concentration of tracer in plasma. In [^{18}F]FDG studies, the vascular compartment, V_{B}, also contributes to the observed concentration in the target tissue $C_{\mathrm{T}}(t)$ (at least for the first frames) and can introduce significant errors in the estimated rate constants if ignored [25, 26]. It is worth noting that each image voxel j has separate rate constants $\boldsymbol{\kappa} = \{\kappa_j\} = [K_{1,j}, k_{2,j}, k_{3,j}, k_{4,j}, V_{B,j}]$ to be estimated. Specifically, during the fth frame the counts within the jth image voxel are equal to:

$$\bar{x}_{fj} = h_{fj}(\boldsymbol{\kappa}) = \frac{1}{t_f^e - t_f^s}\int_{t_f^s}^{t_f^e} C_T(\tau)\mathrm{d}\tau, \qquad \forall f, j, \tag{5}$$

where the total concentration in tissue is equal to $C_{\mathrm{T}}(t) = C_{\mathrm{F}}(t) + C_{\mathrm{B}}(t) + V_{\mathrm{B}}C_{\mathrm{p}}(t)$, t_f^s and t_f^e are start and the end time of frame f and $h_{fj}(\boldsymbol{\kappa})$ is used to denote the overall model that depends on the kinetic parameters $\boldsymbol{\kappa}$.

Spatiotemporal EM framework

The ML estimate of the unknown kinetic parameters $\boldsymbol{\kappa}$, can be calculated by maximising:

$$\hat{\boldsymbol{\kappa}} = \underset{\boldsymbol{\kappa}}{\text{argmax}} \quad l(\boldsymbol{\kappa}|\mathbf{m}), \tag{6}$$

where the Poisson log-likelihood function, given the measured dynamic data $\mathbf{m}$, is given by:

$$l(\boldsymbol{\kappa}|\mathbf{m}) = \sum_{fi}\left(m_{fi}\log_e(\bar{y}_{fi}) - \bar{y}_{fi}\right), \tag{7}$$

where the term $\log_e(m_{fi}!)$ has been dropped as it is not dependent on the kinetic parameters $\boldsymbol{\kappa}$, while the $\bar{y}_{fi}$ is related to the kinetic parameters $\boldsymbol{\kappa}$ through the affine transformation:

$$\bar{y}_{fi} = \sum_j p_{ij}h_{fj}(\boldsymbol{\kappa}) + n_{fi}, \qquad \forall f, i, \tag{8}$$

This problem has been previously solved, for nonlinear two-tissue compartment models, using approaches including iterative coordinate ascent [21] and optimisation transfer [22].

Recently, Matthews et al. [23] proposed a generalised spatiotemporal image reconstruction algorithm, which is a direct implementation of the EM algorithm [27]. The EM algorithm requires the introduction of a set of unobserved 'complete' data, that can be thought of as the intersection between the sinogram and the image space data. As it has been demonstrated by Fessler and Hero [28], the selection of an appropriate 'complete' data formulation is very important, since it can lead to more efficient reconstruction algorithms. Therefore, one option for the 'complete' data $\mathbf{c} = \{c_{fij}\} \in \mathbb{R}^{T\times M\times N}$ is the number of positron emissions from image voxel j, detected in the projection bin i, during the time frame f. It can be shown [23] that the spatiotemporal problem (6) can be decoupled into an image-based ML problem:

$$\boldsymbol{\kappa}^{(k+1)} = \underset{\boldsymbol{\kappa}}{\operatorname{argmax}} \sum_j \left(\sum_i p_{ij} \right) \times \sum_f \left(\bar{x}_{fj}^{(k+1)} \log_e \left(h_{fj}(\boldsymbol{\kappa}) \right) - h_{fj}(\boldsymbol{\kappa}) \right), \quad (9)$$

where the sensitivity image $\sum_i p_{ij}$ acts as a special weight in the maximisation problem and the 'data' $\bar{x}_{fj}^{(k+1)}$ are given by:

$$\bar{x}_{fj}^{(k+1)} = \frac{h_{fj}\left(\boldsymbol{\kappa}^{(k)}\right)}{\sum_i p_{ij}} \sum_i p_{ij} \frac{m_{fi}}{\sum_{j'} p_{ij'} h_{fj'}(\boldsymbol{\kappa}^{(k)}) + n_{fi}}, \quad \forall f, j, \quad (10)$$

which is equivalent to a conventional 3D MLEM reconstruction independently for each dynamic frame. However, in the case of independent models for each image voxel the sensitivity image weight becomes redundant and can be dropped.

Weighted least squares estimation

It can be shown that when the value in the current image estimate $\bar{x}_{fj}^{(k+1)}$ is adequately large, the image-based ML problem (9) can be very well approximated by the image-based weighted least squares (WLS) formulation [23]:

$$\boldsymbol{\kappa}^{(k+1)} = \underset{\boldsymbol{\kappa}}{\operatorname{argmin}} \sum_{fj} w_{fj} \left(\bar{x}_{fj}^{(k+1)} - h_{fj}(\boldsymbol{\kappa}) \right)^2, \quad (11)$$

where the weights, w_{fj}, are derived within the EM framework and are given by the following equation (where the sensitivity image has been dropped):

$$w_{fj} = \frac{1}{h_{fj}(\boldsymbol{\kappa})}, \qquad \forall f, j. \quad (12)$$

However, the weights in (12) cannot be calculated since they depend on the kinetic parameters being optimised. For this reason, a one-step-late (OSL) approach is adopted, where the kinetic parameters are substituted by their expectation calculated in the previous iteration, $\boldsymbol{\kappa}^{(k)}$. Errors caused by this approximation converge to zero, as the estimated kinetic parameters $\boldsymbol{\kappa}^{(k)}$ get closer to the true value.

Likewise, Wang and Qi [22] suggested a formulation for the weights of the WLS problem (equation 26) derived within the optimisation transfer framework. Although the proposed weights are optimal, they are rather complicated, since they depend on the appropriate selection of the curvature of the surrogate function. The transformation of the ML problem (9) into a WLS problem, allows the use of efficient optimisation procedures during the kinetic parameter fitting, such as the non-negative least squares (NNLS) algorithm [29].

Generalised linear least squares

Conventionally, the kinetic parameters of a two-tissue compartment model are estimated by applying a nonlinear regression algorithm on the dynamic PET data. This was also the case in [22], where the Levenberg–Marquardt algorithm was employed. On the contrary, in this work the kinetic parameter vector $\boldsymbol{\kappa}$ is estimated using the NNLS algorithm, after the linearisation of the differential equations (3) and (4) within the GLLS framework [24].

The implementation of the GLLS method adopted the weights described in (12), while the initial estimate for each iterative GLLS procedure was obtained from the previous iteration of the overall reconstruction. Also, it was experimentally found that four internal iterations were enough for the algorithm to converge, without sacrificing computational speed (Fig. 1). Nevertheless, it must be noted that convergence is slower and rather more problematic for very noisy TACs, since it may be trapped in a local minimum. The GLLS algorithm was further optimised for application to clinical data, by pre-calculating the necessary convolution operations and storing them within a library (look-up table) (equation 21 in [24]). During parameter estimation the appropriate value within the look-up table was estimated by linear interpolation. The computational time required for fitting 1000 TACs was approximately 0.43 s (on an Intel^{R} Core^{TM} Duo E8400 3.00 GHz, 12 threads), which is considerably quicker compared to the time required by a nonlinear search algorithm.

Convergence

The proposed algorithm is a direct implementation of the EM framework and, therefore, it guarantees monotonic convergence [23, 27]. However, because the kinetic parameters are nonlinearly related to the measured dynamic PET data, the log-likelihood function (7) is no longer concave with respect to $\boldsymbol{\kappa}$. Therefore, the log-likelihood value will be monotonically increasing with iterations, but it might converge to a local maximum.

Methods

Clinical data

A single [^{18}F]FDG data set was acquired on the HRRT camera, in list-mode over 68 min. The list-mode data were then histogrammed (span 9, ring difference 67) using a scan protocol of 35 frames (1×445 s, 1×30 s, 1×10 s, 12×5 s, 2×10 s, 3×30 s, 3×60 s, 2×120 s,

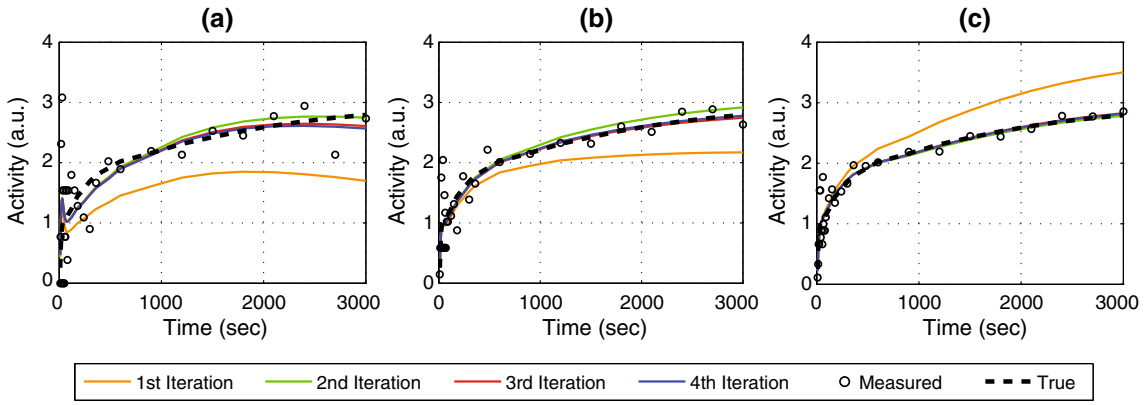

Fig. 1 Simulated examples of fitted TACs using four internal GLLS iterations for different levels of noise (decreasing noise from *left* to *right*). These examples demonstrate that the GLLS algorithm, converges within 4 internal iterations. The *black circles* represent the noisy measurements for each frame, the *dashed line* the true TAC, while the *coloured solid lines* represent the successive fitting attempts

Table 1 Venous samples measured during the scan

Samples	Time post injection (s)	Activity in venous (kBq/mL)
v_1	572	10.76
v_2	995	7.92
v_3	1468	6.82
v_4	2673	4.45
v_5	3572	3.44

10×300 s). The study was approved by the Manchester Independent Research Ethics Committee and by the United Kingdom Administration of Radioactive Substances Advisory Committee.

A population-based input function was calculated by averaging over time six measured arterial input function curves, which were acquired as part of a study to examine [^{18}F]FDG changes with temozolomide changes in cancer patients, and two venous blood samples obtained at 45 and 60 min post injection (Table 1) to scale the population curve to the individual HRRT dataset [30]. Based on the total detected true events (i.e. commonly referred to as the head curve), the input function was corrected for delay, using a spectral analysis model to describe the kinetics [31]. Finally, it was scaled to the acquired data, based on the late venous samples (v_4 and v_5 in Table 1), while the scaling factor was given by Takikawa et al. [32]:

$$sf = \frac{1}{2}\left(\frac{v_4}{p(t_1)} + \frac{v_5}{p(t_2)}\right), \tag{13}$$

where $p(t)$ is the population-based input function and $t_1 = 2673$ s and $t_2 = 3572$ s correspond to the time points where the venous samples were acquired (see Table 1).

The kinetic behaviour of [^{18}F]FDG was modelled as a two-tissue compartment, assuming that the dephosphorylation of FDG during the measurement period is insignificant (i.e. $k_4 = 0$) [33] and including a blood volume (V_B) fraction. In total, four kinetic parameters were calculated, that is, K_1, k_2, k_3 and V_B. In addition, the uptake rate of [^{18}F]FDG, K_i, was calculated by the estimated parameters:

$$K_i = \frac{K_1 k_3}{k_2 + k_3}. \tag{14}$$

The parametric maps were reconstructed using the proposed direct reconstruction algorithm. The tomographic problem (10) was solved using 12 iterations of the ordinary Poisson ordered subsets EM (OP-OSEM) algorithm (16 subsets) [34, 35], while the kinetic modelling step (11) was solved using the GLLS method with 4 internal iterations for each fit. The direct parametric maps were compared with the conventional post-reconstruction parametric maps, which were obtained by independently reconstructing all time frames using an OP–OSEM algorithm (12 iterations, 16 subsets) and then kinetically fitting the TAC of every voxel using the same weights as the direct method within a similar GLLS framework. Both schemes were initialised with a uniform dynamic image estimate (i.e. all ones), although any non-negative initial estimate can be used. However, an initial estimate that is closer to the global optimum (i.e. FBP reconstruction) would not only provide faster convergence [18, 19, 21], but also would allow the algorithm to avoid being trapped in a local optimum.

In addition, because the truth is not known for clinical data, the direct and post-reconstruction parametric maps were also compared, on a region of interest (ROI) basis, to a regularly used and well-established method. Parameters for several predefined ROIs were estimated from the TACs, acquired by reconstructing the data with the filtered back-projection (FBP) algorithm [36], and then fitting them using the nonlinear Levenberg–Marquardt algorithm. Nevertheless, estimation of five parameters is almost

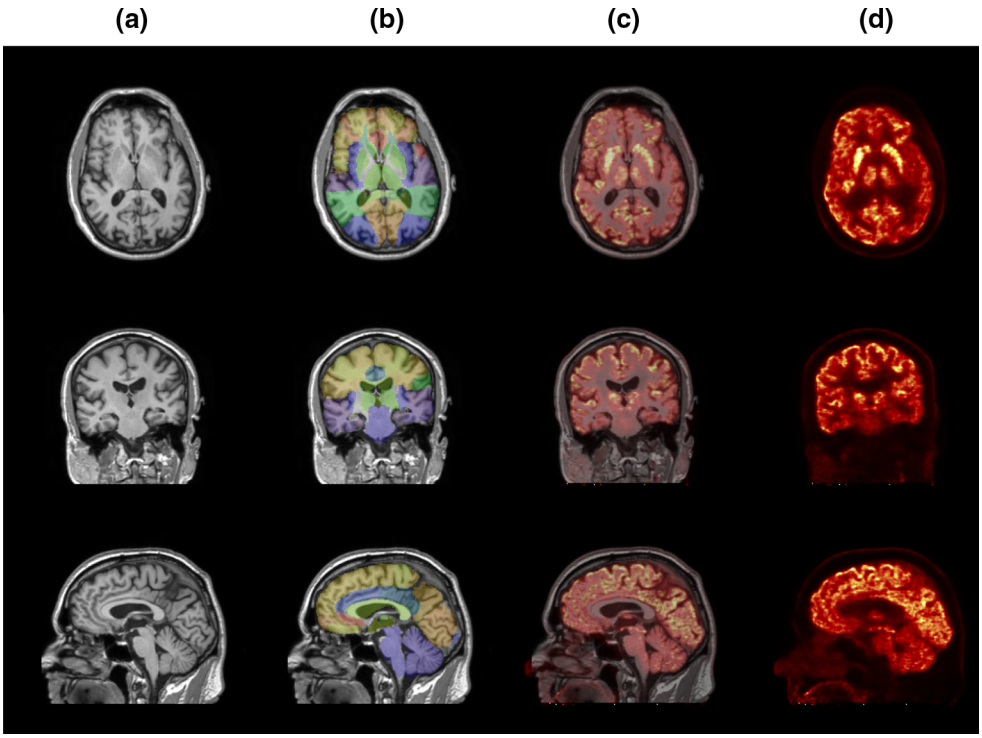

Fig. 2 **a** The magnetic resonance (MR) image; **b** the fused MR image with the *different colours* signifying different regions within the Hammersmith atlas; **c** the fused MR image and the PET image; **d** the PET image

impossible, especially for noisy TACs. Therefore, during the nonlinear fit, the blood volume fraction (V_B) was fixed to 5 % and the k_4 parameter was set equal to a value taken from the literature (i.e. $k_4 = 0.0078$ min^{-1}) [30]. For the rest of this paper, these images will be referred to as 'FBP' and will be considered as the ground truth.

Finally, the uptake rate of [^{18}F]FDG, K_i, which is the parameter with the greatest clinical importance, is conventionally estimated by the Patlak graphical analysis [7]. The method assumes that after a certain period from tracer injection, the concentration of the 'free' tracer is in equilibrium with the concentration in plasma. This assumption leads to the simplification of the original FDG model [33] into a linear equation:

$$\frac{C_T(t_1)}{C_p(t_1)} = \alpha \frac{\int_0^{t_1} C_p(\tau)d\tau}{C_p(t_1)} + \beta, \quad (15)$$

where the slope α represents the tissue uptake rate (i.e. K_i) and the intercept β represents the 'free' tracer fraction in tissue and plasma. The uptake rate is calculated by linear regression including only the later time frames, where the concentration of the unbound tracer is in equilibrium with the concentration in plasma. In this work only the data from 35 min onwards were used (i.e. last 7 frames). Therefore, the parametric maps, acquired with the proposed direct reconstruction method, were also compared to the direct Patlak parametric maps. The model was introduced within the reconstruction, similar to [17, 18], directly estimating two parameters that correspond to the Patlak slope and intercept.

Simulated data

A numerical brain phantom was created by co-registering a maximum probability brain atlas (*Hammersmith atlas* [37, 38]) to the summed PET 3D data, reconstructed with the OSEM algorithm (Fig. 2). The atlas, which consists of 83 brain regions, was used to extract the time activity curves that were then kinetically fitted using the nonlinear Levenberg–Marquardt algorithm (with $V_B = 5$ % and $k_4 = 0.0078$ min^{-1}). The fitted TACs were uniformly assigned back to the corresponding atlas' region, which in turn defined the simulated reference 3D dynamic scan (i.e. true dynamic image).

To simulate the scanner's intrinsic resolution, the dynamic reference scan was smoothed using a Gaussian kernel of 3 mm full width at half maximum (FWHM). Each frame of the blurred reference scan was forward projected to acquire the trues sinogram. Since this sinogram was derived from the reconstructed measured data, a fair assumption is to consider the measured randoms and scatter sinograms as representative measurements and use them in the simulations. Therefore, normalisation and

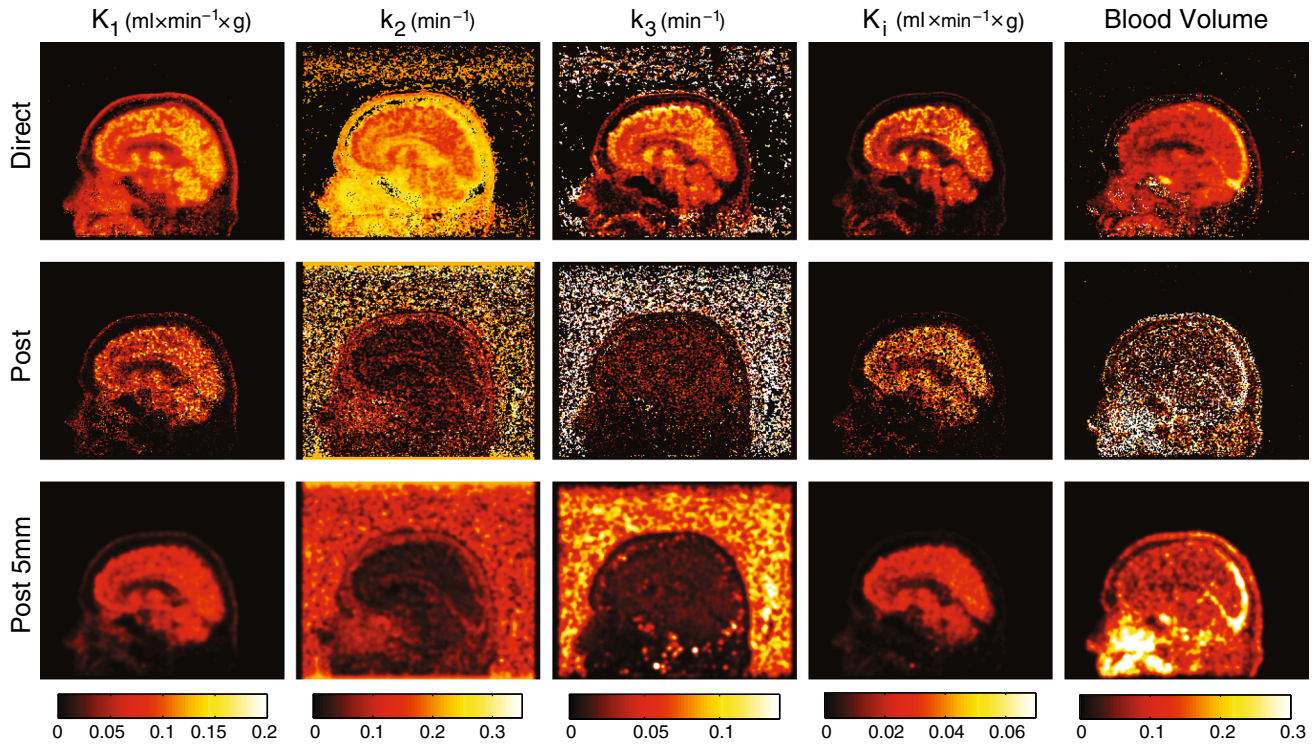

Fig. 3 Parametric maps of the clinical data reconstructed with the proposed direct GLLS reconstruction algorithm (*first row*) and the corresponding post-reconstruction approach (*second row*). Conventionally, to reduce the level of noise in the post-reconstruction parametric maps, the images are also post-smoothed with a Gaussian kernel (5 mm FHWM) prior to kinetic modelling

attenuation effects, as well as the scatter and randoms estimates related to the clinical scan, were introduced in the trues sinogram to obtain the prompts simulated data. Finally, Poisson noise was introduced to match the statistical level of the clinical data, creating a set of 50 noisy realisations.

Similar to the clinical data, the parametric maps were reconstructed using the proposed direct reconstruction algorithm, as well as the corresponding post-reconstruction method. For both cases, the tomographic problem was solved using 12 iterations of the OP-OSEM algorithm (16 subsets) and the kinetic modelling problem was solved using the GLLS method after every subset update.

Since the blood volume fraction (V_B) and the k_4 parameter were fixed during the nonlinear fit of the reconstructed data, the related parametric maps are expected to be uniform (i.e. constant value). For this reason, they are going to be eliminated from the subsequent statistical analysis.

Contrary to the clinical data, the advantage of simulated data, is that the true parametric images are known, for all parametric maps. Based on the true simulated images, estimates of the bias and standard deviation for the reconstructed parametric maps can be calculated across all realisations. In addition, based on the Hammersmith atlas, regional mean bias and standard deviation was calculated for all regions.

Results

Clinical data

Application of the proposed direct reconstruction method to clinical brain [^{18}F]FDG data, showed substantial qualitative improvements, compared to the post-reconstruction method (Fig. 3). Improvements in image quality (i.e. reduced variance) are particularly noteworthy for the k_2 and k_3 micro-parameters, as well as for the estimate of the blood volume fraction (V_B). Additionally, it is interesting to note that for the k_2 and k_3 images, the direct method behaves sufficiently well for those voxels outside the brain. On the contrary, the post-reconstruction method, seems to provide very unstable estimates for the voxels outside of the brain, which cannot be alleviated by post-smoothing the parametric maps.

To evaluate the quantitative accuracy of the parametric reconstruction schemes under investigation the voxel-wise nonlinear fitted FBP image was used as the gold standard. For this reason voxel-wise Bland–Altman plots [39] were

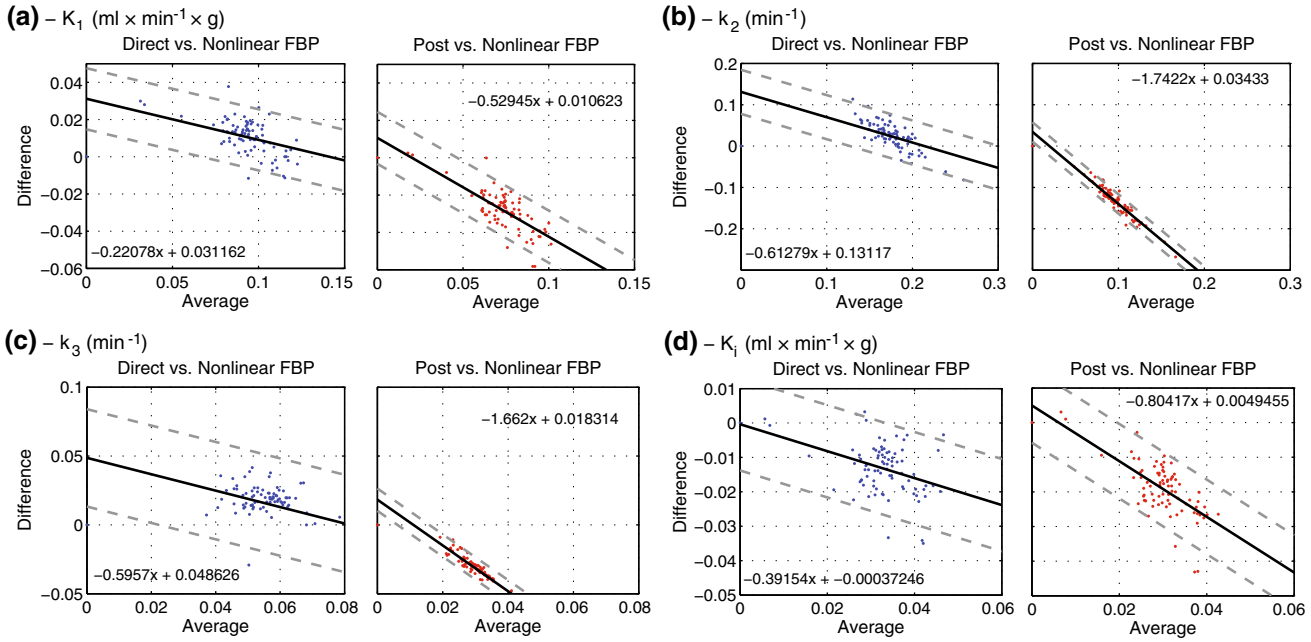

Fig. 4 Region-wise Bland–Altman plots for four parametric maps: **a** K_1, **b** k_2, **c** k_3 and **d** K_i obtained using the clinical data. Each *dot* corresponds to each of the 83 regions of the Hammersmith atlas. The region-wise nonlinear fitted FBP image is used as the gold standard against the proposed direct GLLS reconstruction algorithm (*blue dots*) and the corresponding post-reconstruction parametric approach (*red dots*). The *central line* indicates the linear fit to the data (parameters of the linear fit are shown in the embedded equation), while the outer *dashed lines* indicate the 95 % limits of agreement (±1.96 standard deviation)

Table 2 Coefficients of the fitted line (i.e. slope and intercept) on the Bland–Altman plots

Parameters	Direct		Post-reconstruction	
	Slope	Intercept	Slope	Intercept
K_1	−0.221	0.031	−0.529	0.011
k_2	−0.613	0.131	−1.744	0.034
k_3	−0.596	0.047	−1.662	0.018
K_i	−0.392	0.001	−0.804	0.005

employed to assess the agreement of the mean ROI values within the 83 regions of the Hammersmith atlas obtained with the post-reconstruction and direct reconstruction approaches (Fig. 4). The plots show the difference versus the average between the two methods for each of the 83 regions. The ideal plot should have all points along the zero difference line (indicating exact match), along with small variance between the methods. The linear Bland–Altman fit (Table 2), which can be used as a quantitative metric, reveals consistently better agreement (i.e. smaller slope) between the direct approach and the nonlinear fitted FBP for all parameters for all kinetic parameters. On the other hand, all regions were underestimated by the post-reconstruction method (i.e. negative difference), for every parameter. This is particularly true for the k_2 and k_3 parameters and especially for higher values.

Figure 5 shows the region-wise Bland–Altman plots for the K_i values obtained by (a) the direct reconstruction and (b) the post-reconstruction approaches. Both methods are compared against the well-established direct Patlak method. Similar to previous results, the proposed direct method demonstrates good agreement with the Patlak method, while all mean ROI values are arranged along the zero difference line, with small variance. In contrast, the post-reconstruction method appears to be severely negatively biased with notably higher variance between the estimated values.

Likewise, Fig. 6 shows the voxel-wise scatter plot of the K_i values obtain by (a) the proposed direct method and (b) the post-reconstruction method, as compared to the direct Patlak method, which serves as a gold standard approach. The direct method demonstrated good correlation with the Patlak method where most of the voxels were gathered around the identity line (slope = 1.04, intercept = 1.83×10^{-4}), with an R-squared value equal to $r^2 = 0.9465$. On the other hand, the voxels of the post-reconstruction parametric maps, showed higher variance and smaller correlation to the Patlak method ($r^2 = 0.3547$).

Simulated data

Figure 7 shows the percentage bias versus the standard deviation as a function of iterations for the left posterior

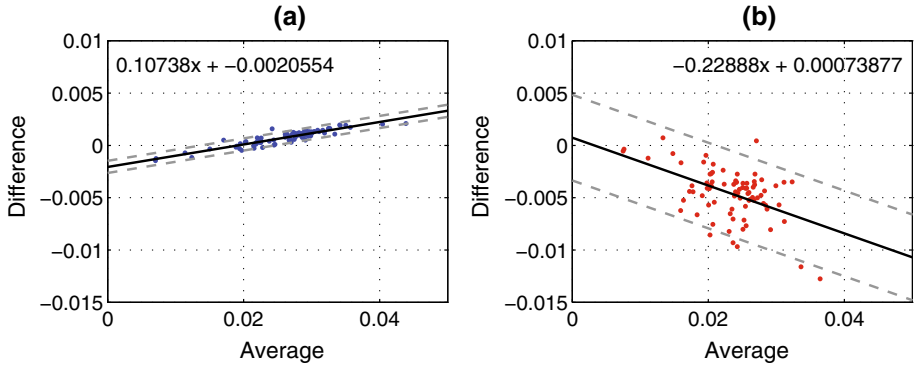

Fig. 5 Region-wise scatter Bland–Altman plots for the K_i parametric map of the clinical data, where each *dot* corresponds to each of the 83 regions of the Hammersmith atlas. In this case the direct Patlak approach is used as the gold standard against: **a** the proposed direct GLLS reconstructed algorithm (*blue dots*) and **b** the corresponding post-reconstruction approached post-smoothed with a 5 mm Gaussian filter (*red dots*). The *central line* indicates the linear fit to the data (parameters of the linear fit are shown in the embedded equation), while the outer *dashed lines* indicate the 95 % limits of agreement (±1.96 standard deviation)

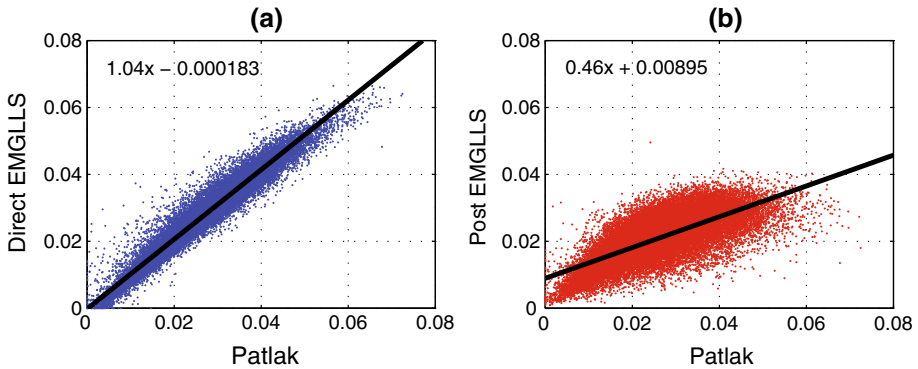

Fig. 6 Voxel-wise scatter plots (approximately 720000 voxels) comparing the K_i values of the clinical data using **a** the proposed direct method and **b** the post-reconstruction method. Both methods are compared against the direct Patlak approach which serves as the gold standard. The R^2 value for the direct method is $r^2 = 0.9465$, while for the post-reconstruction one $r^2 = 0.3547$

temporal lobe, which was considered as a representative region. The post-reconstruction parametric maps suffer from notably high negative bias (up to −80 %), as well as increased standard deviation (from 12 up to 25 %), particularly for late iteration numbers. Similar to the clinical data, the k_2 and k_3 parameters were the most difficult to be estimated, while they demonstrated not only high variance, but also almost doubled bias compared to the K_1 and K_i parameters. On the contrary, direct parametric maps demonstrate lower standard deviation (from 1 up to 8 %) and minimal bias, particularly for the K_1 and K_i parameters. Higher positive bias (up to 30 %) was observed for the k_2 and k_3 parameters, nevertheless it is considerably less compared to the corresponding bias of the post-reconstruction method.

Figure 8 shows the bias images after 12 tomographic iterations. The K_1 parameter, acquired with the direct method, seems to be slightly negatively biased, particularly in the thalamus and on the occipital cortex. In addition, positive bias is observed in the ventricles that can be also seen in the post-reconstruction K_1 image, which apart from this region suffers from high negative bias. Similar results can also be seen for the direct K_i parameter, which is slightly negatively biased, although bias is fairly balanced within the direct reconstructed map. Direct k_2 and k_3 maps generally demonstrate positive bias, with the exception of occipital cortex and thalamus for the k_2 and the ventricles for the k_3, where bias appears to be negative. Post-reconstruction k_2 and k_3 maps are severely negatively bias throughout the image.

Figure 9 shows the standard deviation (%) images after 12 tomographic iterations. Directly reconstructed K_1 and K_i maps demonstrated the lowest standard deviation, while the worst has been demonstrated by the post-reconstructed k_2 and k_3 maps. Generally, all post-reconstruction maps were outperformed by the direct maps, with differences being more pronounced for the challenging k_2 and k_3 micro-parameters.

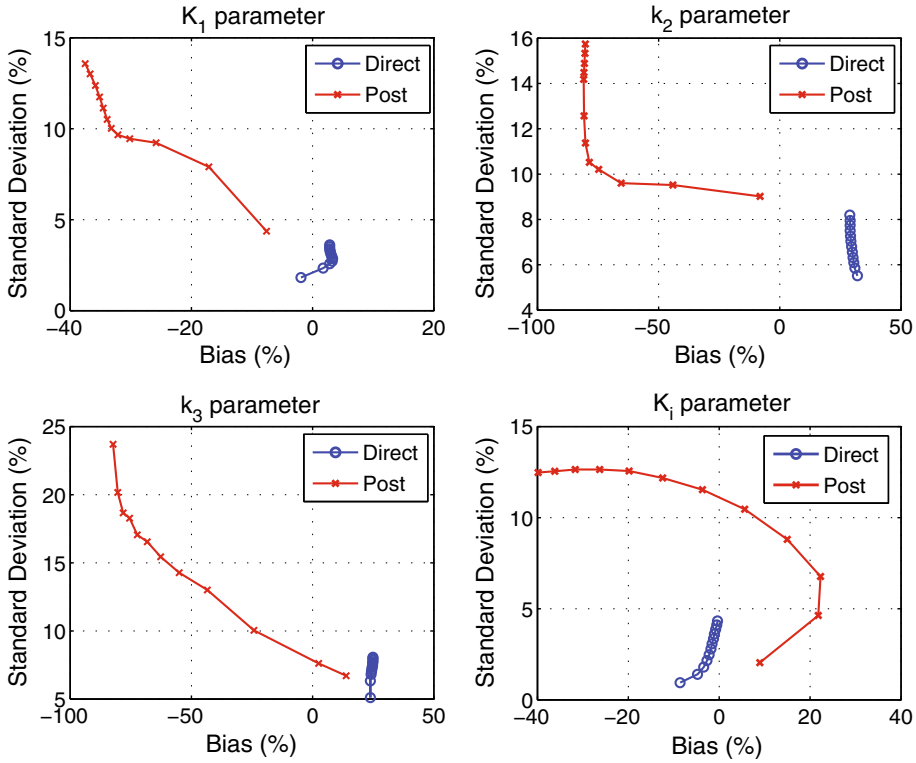

Fig. 7 Mean bias (%) versus standard deviation (%) curves, across 50 realisations, of the simulated data. The *curves* correspond to a representative region acquired from the Hammersmith atlas (i.e. left posterior temporal lobe). Each *point* represents a tomographic iteration up to 12 and as iterations increase variance increases for all cases

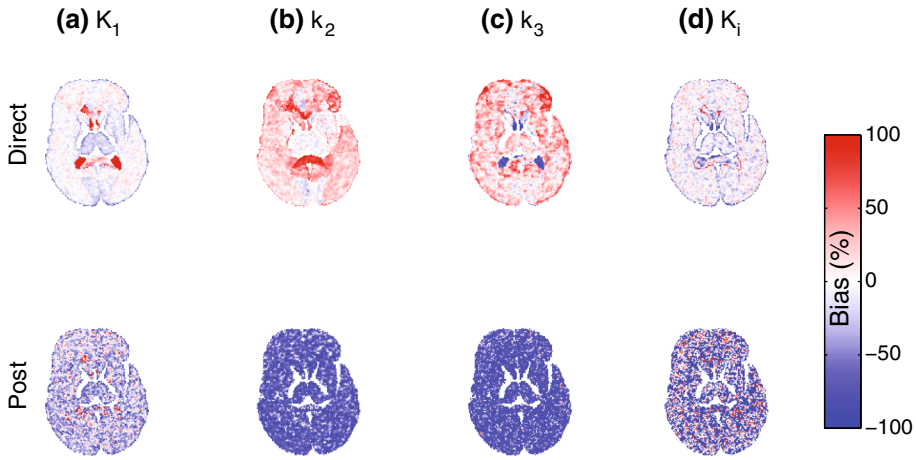

Fig. 8 Bias images (percentage over the true value) for the direct (*upper row*) and post-reconstruction approaches (*lower row*). The parametric images were obtained after 12 tomographic iterations and were based on 50 realisations of simulated data

Discussion

Parametric image reconstruction, based on a two-tissue compartment model, is a rather challenging and computationally intensive task, when all individual kinetic parameters are to be estimated [21, 22, 40]. Often, nonlinear optimisation procedures are employed to estimate these micro-parameters, which are rather impractical in a voxel-by-voxel estimation scenario, since they lead to overall very long reconstruction times. For this reason, many studies have been limited to estimating macro-parameters, which are often derived from graphical analysis methods, using linear regression procedures [17, 18]. In this paper, the generalised linear least squares framework was exploited within a recently proposed direct parametric reconstruction algorithm [23, 41], to linearise the operational equation of a two-tissue compartment model and yet maintain the estimation of all individual micro-parameters [24].

In contrast to similar methods which employ rather complicated weights derived within a separable surrogate function framework (e.g. [22]), the proposed method uses simple weighting factors for the least squares objective function that were naturally derived within an expectation

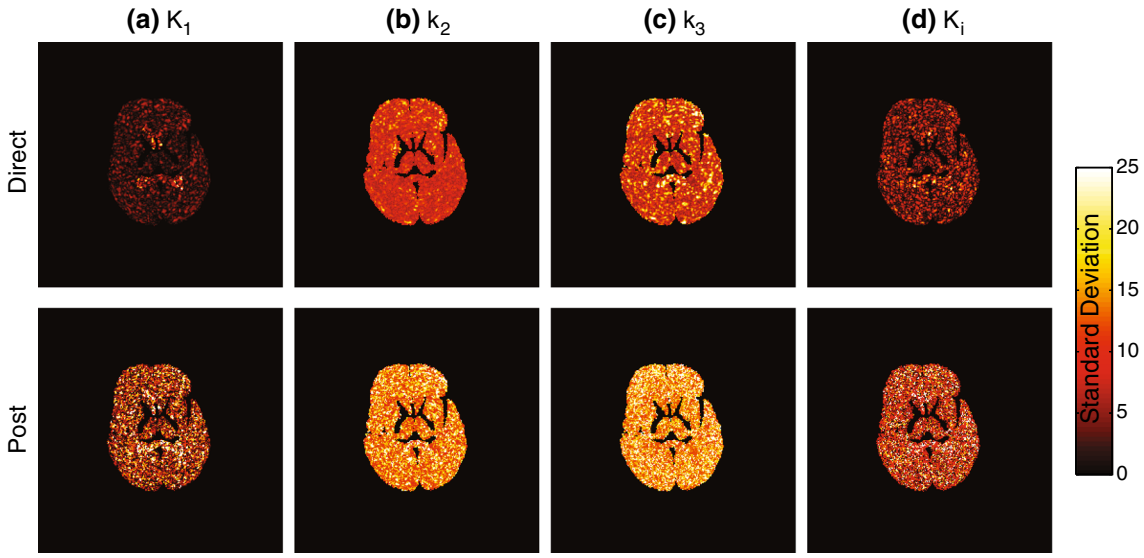

Fig. 9 Standard deviation images (percentage over the true value) for the direct (*upper row*) and post-reconstruction methods (*lower row*). The parametric images were obtained after 12 tomographic iterations and were based on 50 realisations of simulated data

maximisation framework. The weights, which were updated at each internal GLLS iteration, were based on the expectation of the kinetic parameters at the previous iteration, similar to a one-step-late approach. The employed weights were particularly appropriate for the proposed direct reconstruction algorithm, as the previous image estimate is always available (except for the first iteration, where approximations based on the frame duration can be used). On the other hand, the same weighting factors are not suitable for the conventional post-reconstruction approach, since (usually) the previous estimate is not available. Contrary to the direct approach, where the weights were updated at each iteration using a temporal constraint, the weighting factors used by the post-reconstruction approach tend to be fairly noisy. Therefore, they cannot appropriately describe the noise distribution in the reconstructed images [42], leading to suboptimal parameter estimation.

It is worth noting that in this work four internal GLLS iterations were used for each fitting step. Too few internal iterations might lead to a suboptimal fit (Fig. 1), while more internal iterations add unnecessary computational burden to the overall reconstruction time. The optimal number of internal iterations depends on two factors: (a) the initial estimate for the weights and (b) the level of noise in the TAC to be fitted. The proposed direct reconstruction method is better than the post-reconstruction method in both regards. Firstly, the direct method uses the previously fitted TAC as the initial estimate for the weights, while the post-reconstruction method uses the current reconstructed TAC which tends to be very noisy (hence less optimal). Secondly, because the direct method fits the TAC at each iteration, it leads to less noisy TACs compared to the post-reconstruction approach, particularly for late tomographic iterations. This means that the direct method usually requires fewer internal GLLS iterations—often less than four (see Fig. 1)—which takes considerably less time compared to a nonlinear fit.

In terms of computational complexity, the direct and the post-reconstruction approaches share the same tomographic algorithm and the same parameter fitting procedure. For the post-reconstruction approach parameter fitting is performed only once, at the end of the reconstruction, while for the direct approach it is applied after every subset update. Therefore, since there is no additional computational overhead between the two approaches the difference in the overall reconstruction time is proportional to the total number of iterations. This is only because the GLLS procedure is applied more times compared to the post-reconstruction method. However, although this multiple fitting of the TACs adds a considerable computational burden, it leads to improved parameter estimates.

Application of the proposed direct reconstruction method to clinical data acquired on the HRRT scanner, showed apparent improvements in image quality for all micro-parameters, compared to the conventional post-reconstruction method and the corresponding post-filtered images (Fig. 3). Directly reconstructed images appeared not only smoother, but also structural information was available, in the brain cortex, thalamus, as well as cerebellum. On the contrary, such information was not present in the post-reconstruction parametric images due to the increased noise. In addition, functional information was different between the two methods, especially for the K_1

and blood volume images. Increased uptake rate was observed in the sinus area for the direct K_1 parameter, which is something to be expected. However, this information was not resolved in the post-reconstructed K_1 image, while increased activity was assigned to the same area in the blood volume parameter (Fig. 3). This can be explained by the inability of the post-reconstruction method to determine the correct uptake rate (and consequently blood volume) due to increased noise in the early short frames.

Since, the ground truth is not known for clinical data, the proposed direct reconstruction approach was compared against two well-established methods. Region-wise comparison to the FBP reconstructed images followed by nonlinear fitting using the Levenberg–Marquardt algorithm showed adequate agreement for all micro-parameters (Fig. 4). This was especially true for the K_1 and K_i parameters, which were slightly underestimated, probably due to the absence of the k_4 parameter from the employed kinetic model (see Sect. 3.1). On the other hand, excellent quantitative agreement was observed when the proposed direct reconstruction method was compared against the direct Patlak method (Fig. 5). This can be partly attributed to the same assumption about the k_4 parameter that is employed by the Patlak model and the proposed method, since both approaches assumed that the dephosphorylation of FDG is negligible. On the contrary, post-reconstructed parametric maps showed substantial disagreement when compared to nonlinear fitted FBP images, particularly for the k_2 and k_3 parameters.

The trends in variance observed in the reconstructed parametric maps based on clinical data, were replicated in the reconstructed images using simulated [^{18}F]FDG data. Post-reconstruction parametric maps suffered from increased standard deviation particularly for the k_2 and k_3 parameters, while parametric maps reconstructed with the direct approach demonstrated notably lower standard deviation (i.e. 2–3 times less) (Fig. 7). However, apart from improvements in noise properties, the proposed direct method also demonstrated lower bias for all micro-parameters. Likewise, the most difficult parameters to estimate accurately were k_2 and k_3, where the bias reached 30 % compared to 80 % for the post-reconstruction approach. On the contrary, the macro-parameters K_1 and K_i were estimated with negligible bias, which did not exceed 5 % (Fig. 7). The large negative bias observed for the post-reconstruction parametric maps could possibly be explained by the inability of the algorithm to handle very noisy data. It has been shown [5] that the performance of the GLLS algorithm rapidly deteriorates with increasing levels of noise in the TACs and tends to be trapped in local minima. Introducing a spatial regularisation within the tomographic step (e.g. median root prior, quadratic prior) can improve the noise characteristics in the reconstructed images and, therefore, potentially offer improvements in accuracy, at least for the post-reconstruction approach [43].

In this work, the dephosphorylation of [^{18}F]FDG was assumed to be negligible (i.e. zero) [33]. Although there is a controversy about the validity of this assumption [44, 45], it was employed in this work, mainly to reduce the number of estimated parameters. Since the k_4 parameter is the most difficult parameter to estimate, it is expected that it will also affect the estimation of the other micro-parameters. Inclusion of the k_4 parameter will result in the model being more accurate, thus reducing the observed bias in the estimated parameters. Nevertheless, it is expected that introduction of an additional parameter will also lead to greater instability (i.e. higher variance). Therefore, it is recommended to estimate only four micro-parameters, including the blood volume fraction, and assume that the k_4 parameter is zero (or a fixed value). However, it must be noted that within a 4D framework, errors due to potential model mismatch triggered by incorrect assumptions about the kinetic parameters (e.g. negligible k_4 or fixed V_B) may propagate to neighbouring well-modelled regions and affect the overall quantification of the reconstructed parameters [26, 46].

One limitation of this work is that the performance of the proposed direct reconstruction method was not compared, in terms of its bias and variance properties, to existing direct methods, such as the ones presented in [21, 22]. This investigation is fairly necessary to clearly demonstrate the strengths and weaknesses of the proposed method. However, the purpose of this paper was to introduce and evaluate the generalised direct reconstruction algorithm initially proposed by Matthews et al. [23] in the context of nonlinear models and demonstrate the advantages over the corresponding conventional post-reconstruction method [41]. Future work should include more elaborate simulations, where the proposed method and the above mentioned methods will be compared in terms of their bias-variance trade-off, as well as their computational complexity. In addition, different reconstruction methods have diverse characteristics in terms of quantitative errors and signal-to-noise ratio. Although iterative methods offer better images in terms of resolution and signal-to-noise ratio, FBP algorithms are considered to offer better quantification, particularly for low-count regions. Such quantification errors can be very important for the end-point biological parameters. Therefore, a comprehensive comparison, in terms of quantification, of the proposed direct reconstruction method against the conventional post-reconstruction FBP approach would be necessary. On the other hand, maximum a posteriori algorithms apply some form of regularisation to

stabilise the image estimates, thus leading to improved noise characteristics. This could potentially reduce the excess variance of the post-reconstruction EM approach and improve all parameter estimates.

In general, the proposed direct parametric reconstruction algorithm demonstrated not only improvements in precision (i.e. lower variance), but also in accuracy (i.e. lower bias) when compared to the conventional post-reconstruction method. High resolution parametric images were reconstructed, with high contrast between gray and white matter, while structural information was visible. As expected, the best performance was observed for the estimation of the macro-parameters K_1 and K_i, which was comparable to the well-established direct Patlak method [17, 18], at least for the K_i parameter. However, the advantage of this method over the well-established graphical analysis method is that it can also provide the micro-parameters with acceptable accuracy and precision.

Conclusions

In this paper we presented and evaluated an expectation maximisation parametric reconstruction algorithm for estimating the micro-parameters of a two-tissue compartment model directly from the measured PET data. The method was applied to simulated and clinical [^{18}F]FDG data acquired on the high resolution research tomograph. Computer simulations showed that the direct method demonstrated superior performance over the conventional post-reconstruction method both in quantitative accuracy and precision, for all micro-parameters. Considerable improvements in image quality were observed for clinical data, whilst showing reasonable agreement with the well-established FBP post-reconstructed images.

References

1. Ichise M, Meyer JH, Yonekura Y. An introduction to PET and SPECT neuroreceptor quantification models. J Nucl Med. 2001;42(5):755–63.
2. Schmidt KC, Turkheimer FE. Kinetic modeling in positron emission tomography. Q J Nucl Med. 2002;46(1):70–85.
3. Bentourkia M, Zaidi H. Tracer kinetic modeling in PET. PET Clin. 2007;2(2):267–77.
4. Gunn RN, Gunn SR, Cunningham VJ. Positron emission tomography compartmental models. J Cerebr Blood Flow Metab. 2001;21(6):635–52.
5. Dai X, Chen Z, Tian J. Performance evaluation of kinetic parameter estimation methods in dynamic FDG-PET studies. Nucl Med Commun. 2011;32(1):4–16.
6. Marquardt DW. An algorithm for least-squares estimation of nonlinear parameters. SIAM J Appl Math. 1963;11(2):431–41.
7. Patlak CS, Blasberg RG, Fenstermacher JD. Graphical evaluation of blood-to-brain transfer constants from multiple-time uptake data. J Cerebr Blood Flow Metab. 1983;3(1):1–7.
8. Logan J, Fowler JS, Volkow ND, Wolf AP, Dewey SL, Schlyer DJ, et al. Graphical analysis of reversible radioligand binding from time-activity measurements applied to [N-^{11}C-methyl]-(-)-cocaine PET studies in human subjects. J Cerebr Blood Flow Metab. 1990;10(5):740–7.
9. Turkheimer FE, Aston JA, Asselin MC, Hinz R. Multi-resolution Bayesian regression in PET dynamic studies using wavelets. NeuroImage. 2006;32(1):111–21.
10. Slifstein M, Laruelle M. Effects of statistical noise on graphic analysis of PET neuroreceptor studies. J Nucl Med. 2000;41(12):2083–8.
11. Kimura Y, Naganawa M, Shidahara M, Ikoma Y, Watabe H. PET kinetic analysis—pitfalls and a solution for the Logan plot. Ann Nucl Med. 2007;21(1):1–8.
12. Tsoumpas C, Turkheimer FE, Thielemans K. A survey of approaches for direct parametric image reconstruction in emission tomography. Med Phys. 2008;35(9):3963–71.
13. Rahmim A, Tang J, Zaidi H. Four-dimensional (4D) image reconstruction strategies in dynamic PET: beyond conventional independent frame reconstruction. Med Phys. 2009b;36(8):3654–70.
14. Matthews JC, Bailey D, Price P, Cunningham VJ. The direct calculation of parametric images from dynamic PET data using maximum-likelihood iterative reconstruction. Phys Med Biol. 1997;42(6):1155–73.
15. Meikle SR, Matthews JC, Cunningham VJ, Bailey DL, Livieratos L, Jones T, et al. Parametric image reconstruction using spectral analysis of PET projection data. Phys Med Biol. 1998;43(3):651–66.
16. Wang G, Qi J. Acceleration of the direct reconstruction of linear parametric images using nested algorithms. Phys Med Biol. 2010;55(5):1505–17.
17. Wang G, Fu L, Qi J. Maximum a posteriori reconstruction of the Patlak parametric image from sinograms in dynamic PET. Phys Med Biol. 2008;53(3):593–604.
18. Tsoumpas C, Turkheimer FE, Thielemans K. Study of direct and indirect parametric estimation methods of linear models in dynamic positron emission tomography. Med Phys. 2008;35(4):1299–309.
19. Angelis GI, Thielemans K, Tziortzi AC, Turkheimer FE, Tsoumpas C. Convergence optimization of parametric MLEM reconstruction for estimation of Patlak plot parameters. Comput Med Imaging Graphics. 2011;35(5):407–16.
20. Rahmim A, Zhou Y, Tang J, Wong DF. Direct 4D parametric image reconstruction with plasma input and reference tissue models in reversible binding imaging. In: IEEE Nucl Sci Symp Conf Rec, NSS/MIC 2009; 2009. p. 2516–22.
21. Kamasak ME, Bouman CA, Morris ED, Sauer K. Direct reconstruction of kinetic parameter images from dynamic PET data. IEEE Trans Med Imag. 2005;24(5):636–50.
22. Wang G, Qi J. Generalized algorithms for direct reconstruction of parametric images from dynamic PET data. IEEE Trans Med Imag. 2009;28(11):1717–26.
23. Matthews JC, Angelis GI, Kotasidis FA, Markiewicz PJ, Reader AJ. Direct reconstruction of parametric images using any spatiotemporal 4D image based model and maximum likelihood expectation maximization. IEEE Nucl Sci Symp Conf Rec NSS/MIC. 2010;M10–6(2010):2435–41.
24. Feng D, Ho D, Chen K, Wu LC, Wang JK, Liu RS, et al. Evaluation of the algorithms for determining local cerebral metabolic rates of glucose using positron emission tomography dynamic data. IEEE Trans Med Imag. 1995;14(4):697–710.

25. Wienhard K, Pawlik G, Herholz K. Estimation of local cerebral glucose utilization by positron emission tomography of [^{18}F]2-fluoro-2-deoxy-D-glucose: A critical appraisal of optimization procedures. J Cerebr Blood Flow Metab. 1985;5(1):115–25.
26. Tsoumpas C, Thielemans K. Direct parametric reconstruction from dynamic projection data in emission tomography including prior estimation of the blood volume component. Nucl Med Commun. 2009;30(7):490–3.
27. Dempster AP, Laird NM, Rubin DB. Maximum likelihood from incomplete data via the EM algorithm. J R Stat Soc Ser B. 1977;39(1):1–38.
28. Fessler JA, Hero AO. Space-alternating generalized expectation-maximization algorithm. IEEE Trans Signal Process. 1994; 42(10):2664–77.
29. Lawson CL, Hanson RJ. Solving least squares problems. 3rd ed. Englewood Cliffs: Prentice-Hall; 1974.
30. Phillips RL, Chen CY, Wong DF, London ED. An improved method to calculate cerebral metabolic rates of glucose using PET. J Nucl Med. 1995;36(9):1668–79.
31. Hinz R, Turkheimer FE. Determination of tracer arrival delay with spectral analysis. IEEE Trans Nucl Sci. 2006;53(1):212–9.
32. Takikawa S, Dhawan V, Spetsieris P, Robeson W, Chaly T, Dahl R, et al. Noninvasive quantitative fluorodeoxyglucose PET studies with an estimated input function derived from a population-based arterial blood curve. Radiology. 1993;188(1):131–6.
33. Sokoloff L, Reivich M, Kennedy C. The [^{14}C]deoxyglucose method for the measurement of local cerebral glucose utilization: theory, procedure, and normal values in the conscious and anesthetized albino rat. J Neurochem. 1977;28(5):897–916.
34. Politte DG, Snyder DL. Corrections for accidental coincidences and attenuation in maximum-likelihood image reconstruction for positron-emission tomography. IEEE Trans Med Imag. 1991; 10(1):82–9.
35. Hudson HM, Larkin RS. Accelerated image reconstruction using ordered subsets of projection data. IEEE Trans Med Imag. 1994;13(4):601–9.
36. Van Velden FHP, Kloet RW, Van Berckel BNM, Wolfensberger SPA, Lammertsma AA, Boellaard R. Comparison of 3D-OP-OSEM and 3D-FBP reconstruction algorithms for high-resolution research tomograph studies: effects of randoms estimation methods. Phys Med Biol. 2008;53(12):3217–30.
37. Hammers A, Allom R, Koepp MJ, Free SL, Myers R, Lemieux L, et al. Three-dimensional maximum probability atlas of the human brain, with particular reference to the temporal lobe. Hum Brain Mapp. 2003;19(4):224–47.
38. Gousias IS, Rueckert D, Heckemann RA, Dyet LE, Boardman JP, Edwards AD, et al. Automatic segmentation of brain MRIs of 2-year-olds into 83 regions of interest. NeuroImage. 2008;40(2): 672–84.
39. Bland JM, Altman DG. Measuring agreement in method comparison studies. Stat Methods Med Res. 1999;8(2):135–60.
40. Tsoumpas C, Turkheimer F, Thielemans K. Convergence properties of algorithms for direct parametric estimation of linear models in dynamic PET. In: IEEE Nucl Sci Symp Conf Rec; 2007. p. 3034–7.
41. Angelis GI, Matthews JC, Kotasidis FA, Markiewicz PJ, Lionheart WR, Reader AJ. Evaluation of a direct 4D reconstruction method using GLLS for estimating parametric maps of microparameters. In: IEEE Nucl Sci Symp Conf Rec, NSS/MIC; 2012. p. 2355–9.
42. Barrett HH, Wilson DW, Tsui BM. Noise properties of the EM algorithm: I. Theory Phys Med Biol. 1994;39(5):833–46.
43. Tsoumpas C, Polycarpou I, Thielemans K, Buerger C, King AP, Schaeffter T, et al. The effect of regularization in motion compensated PET image reconstruction: a realistic numerical 4D simulation study. Phys Med Biol. 2013;58(6):1759–73.
44. Phelps ME, Huang SC, Hoffman EJ. Tomographic measurement of local cerebral glucose metabolic rate in humans with (F-18)2-fluoro-2-deoxy-D-glucose: Validation of method. Ann Neurol. 1979;6(5):371–88.
45. Hong YT, Fryer TD. Kinetic modelling using basis functions derived from two-tissue compartmental models with a plasma input function: General principle and application to [18F]fluorodeoxyglucose positron emission tomography. NeuroImage. 2010;51(1):164–72.
46. Kotasidis FA, Matthews JC, Angelis GI, Markiewicz PJ, Lionheart WR, Reader AJ. Impact of erroneous kinetic model formulation in direct 4D image reconstruction. In: IEEE Nucl Sci Symp Conf Rec; 2012. p. 2366–7.